

A Novel Self-supporting GEM-based Amplification Structure for a Time Projection Chamber at the ILC

2

3

Ties Behnke^a, Ralf Diener^a, Christoph Rosemann^a, Lea Steder^{a*}

^aDESY,

Notkestrasse 85, 22607 Hamburg, Germany

E-mail: lea.steder@desy.de

4

ABSTRACT: In this paper, a new self-supporting way to mount Gas Electron Multiplier on readout boards is presented. It has been developed to cover large readout areas while ensuring the flatness of the Gas Electron Multiplier foils and keeping the amount of material and the dead zone minimal. The structure has been tested in a Time Projection Chamber prototype, using cosmic muon tracks. The impact of the mounting structure on the charge measurement, the track reconstruction and the single point resolution is quantified.

5

KEYWORDS: Micropattern gaseous detectors (MSGC, GEM, THGEM, RETHGEM, MHSP, MICROPIC, MICROMEGAS, InGrid, etc); Time projection Chambers (TPC); Detector design and construction technologies and materials; Overall mechanics design.

6

7

8

*Corresponding author

Contents	10
1. Introduction	1 11
2. Design, Material and Flatness of Grid GEMs	2 12
3. Experimental Setup for Studies of a Grid GEM TPC with Cosmic Muon Data	4 13
4. Grid Impact on Charge Measurement	5 14
5. Grid Impact on Hit Reconstruction and Hit Efficiencies	6 15
6. Impact of the Grid on the Track Reconstruction	8 16
7. Conclusion	11 17

1. Introduction 19

A Time Projection Chamber (TPC) is envisaged as the main tracking detector of the International Large Detector (ILD) [1], [2]. The requirements on the design of the ILD TPC are driven by the particle flow concept —described in [1]— and the high precision physics measurements planned at the International Linear Collider (ILC). In table 1, the design parameters for the ILD TPC are listed. Most important are the momentum resolution, a very good hit and track efficiency and the limited amount of material —respectively radiation length— in front of the calorimeters as well as the good hermiticity.

A TPC combines a large number of measurement points with good resolution in three dimensions. This ensures a very robust and efficient pattern recognition. The amplification and readout system for such a TPC needs to provide a large area coverage while introducing a minimum of insensitive regions to allow for a very high particle reconstruction efficiency, i.e. good hit and track reconstruction efficiencies. Further, the required momentum resolution of $\delta(1/p_T) \simeq 1 \times 10^{-4} / (\text{GeV}/c)$ — which translates into a single point resolution of 100 μm in the $r\phi$ -plane [1]— has to be achieved. Finally, uniform effective gains have to be ensured to allow for precise dE/dx measurements. Therefore, the flatness of the amplification device has to be guaranteed by the mechanical design of the structure. Here GEM (Gas Electron Multiplier) foils [3] are used, but within the ILD concept also other possibilities for signal amplification like MICROMEAS [4] or InGrid [5] are under study. The support structure described in this paper consists of a light-weight ceramic grid, which ensures a constant distance between the different GEM layers. The grid is glued to the GEM so that the system becomes mechanically stable and scalable to varying numbers of GEMs. With the size of the grid cell size properly chosen, the structure ensures a flat amplification system, which is self-supporting and can be easily mounted on a readout plane with minimal dead zones.

Table 1. Performance and design parameters for the TPC with standard electronics and pad readout as defined in the ILD Detailed Baseline Document [2].

Parameter	r_{in}	r_{out}	Z
Geometrical parameters	329 mm	1808 mm	± 2350 mm
Solid angle coverage	Up to $\cos\theta \simeq 0.98$ (10 pad rows)		
TPC material budget	$\simeq 0.05 X_0$ including outer fieldcage in r $< 0.25 X_0$ for readout endcaps in z		
Number of pads/timebuckets	$\simeq 1-2 \times 10^6/1000$ per endcap		
Pad pitch/ no.padrows	$\simeq 1 \times 6$ mm ² for 220 padrows		
σ_{point} in $r\phi$	$\simeq 60$ μ m for zero drift, < 100 μ m overall		
σ_{point} in rz	$\simeq 0.4 - 1.4$ mm (for zero – full drift)		
2-hit resolution in $r\phi$	$\simeq 2$ mm		
2-hit resolution in rz	$\simeq 6$ mm		
dE/dx resolution	$\simeq 5$ %		
Momentum resolution at B=3.5 T	$\delta(1/p_T) \simeq 10^{-4}/(\text{GeV}/c)$ (TPC only)		

In the following, the design of the support system is described and its impact on the performance of the GEM readout in terms of hit efficiency, tracking performance and single point resolution is studied.

2. Design, Material and Flatness of Grid GEMs

In this section, a new concept to support GEMs with a ceramics grid is introduced. This structure ensures constant transfer and induction gaps in between the GEM foils. The gaps inside the GEM stack are called transfer regions, while the gap between last GEM foil and readout board is mentioned as induction region.

The support structure is made of an aluminum oxide ceramic (Al_2O_3) [6]. This material is very stiff, an excellent insulator and machinable by laser cutting. A technical drawing of the grids, which were produced to hold standard 10×10 cm² GEMs in a TPC prototype at DESY [7], can be seen in figure 1(a). The relevant characteristics are summarized in table 2. The advantage of the grid support is the almost edgeless mounting, which provides the possibility to mount two grid modules very close to each other with only a minimal gap of dead material in between. In addition, the optical transparency as ratio of uncovered to total sensitive area is about 96 %. The outer dimensions of the grid are chosen to fit in a medium size TPC prototype. The restriction to the ratio 1 : 1 for width and height of the bars is given by the current production process. In order to achieve a width of only 1 mm, but a height of 2 mm, which is needed to provide sufficiently large transfer gaps in the GEM stack, two grids were glued on top of each other.

A triple grid GEM stack was produced by gluing GEM foils directly onto the grids with a two-component epoxy resin glue (polybond EP 4619/3 [9]). The grid is only glued on the outer bars to avoid glue stains on the sensitive GEM area. A stretching via heating of the foils is—in contrast to the traditional frame mounting—not necessary. This permits the mounting structure to be thin,

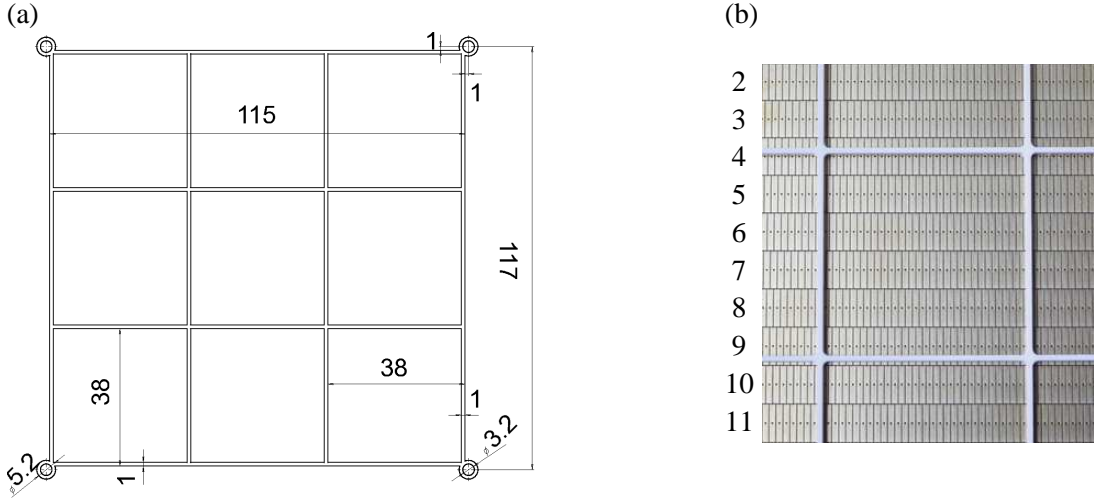


Figure 1. (a) Drawing of ceramics grid, [8]. All measures are given in millimeters. (b) Relative position of grid and pad plane. Row one and twelve are also in the sensitive area of the GEM foils, but not connected due to a limited amount of available readout channels.

Table 2. Material properties and dimensions of grid support structure.

grid support measures	
material	Al_2O_3
radiation length	$X_0 = 7.0 \text{ cm}$
resistivity	$> 10^{12} \Omega\text{cm}$
bending strength	$\sigma_B = 350 \text{ MPa}$
outer dimensions	$117 \times 117 \text{ mm}^2$
cell size	$37 \times 37 \text{ mm}^2$
sensitive GEM area	$10 \times 10 \text{ cm}^2$
optical transparency	96 %
structure width	1 mm
structure height	1 mm

since only small mechanical forces have to be absorbed. 65

The assembled GEM stack is placed on a readout plane instrumented with pads with an area of $1.27 \times 7 \text{ mm}^2$, shown in figure 1(b). Adjacent rows of pads are staggered by half a pad pitch and the grid is aligned to the pads. The sensitive region of the readout plane is about $61 \times 70 \text{ mm}^2$. 66 67 68

To study the impact of the grid on the tracking performance, it was placed above a normal pad plane. The complete area, including the pads directly below the grid structure, is instrumented. For the given pad and grid mesh size, in total, about 26 % of the pads are partly covered by the grid. Therefore, it is essential to study the impact the grid has on the performance and to determine the impact on pads directly beneath and adjacent to the grid structure. 69 70 71 72 73

The radiation length of aluminum oxide (7 cm, cf. table 2) has to be compared to $X_0 = 19.4 \text{ cm}$ for glass fiber reinforced plastic (GRP) [10]. However, the bending strength of the ceramic grid allows the surface of the support structure to be built significantly smaller compared to the GRP surface of the traditional mounting frames, which have a width of 10 mm. The finer grid structures result 74 75 76 77

in five times less dead material inside the detector assuming a triple GEM structure and compared to the conventional GEM mounting.

An additional advantage of the new procedure is the flatness of the mounted GEM foils. In [11], a detailed study of conventionally mounted GEM surface profiles is presented. For this purpose eight GRP framed and stretched GEM surface profiles were measured and quantified with their maximal height deviations Δz . This variable varies for the eight GEMs between 384 μm and 922 μm [11]. A parametrization of charge transfers in GEM amplification stacks described in [12] allows simulation of effective gains. Using this simulation in combination with the measured surface profiles, the gain uniformity for tracks over the readout of a TPC prototype are studied in [11].

Here, only the results of this analysis are quoted and can be summarized in stating, that a flat mounting of GEMs with a $\Delta z < 600 \mu\text{m}$ is necessary in order to reach the required dE/dx resolution of smaller than five percent for the ILD TPC [1]. Only half of the framed GEMs measured in [11] meet the flatness requirements. The GEM profiles mounted with the new grid structure were also measured and both surfaces fulfill the demands for the gain uniformity with a Δz of 385 μm respectively 514 μm , although no thermal stretching was applied during the gluing process. For the mounting procedure with GRP frames, such a stretching is needed. Within the limits of the available statistics, it can therefore be stated, that the grid structure ensures besides its other advantages a sufficiently flat mounting.

3. Experimental Setup for Studies of a Grid GEM TPC with Cosmic Muon Data

For the studies, a triple grid GEM stack composed of $10 \times 10 \text{ cm}^2$ GEMs (double conical holes, hole pitch 140 μm , 50/70 μm inner/outer hole diameter) was constructed with the ceramic grids. The stack was operated in a prototype TPC with an inner diameter of 27 cm and drift length of 66 cm at magnetic fields of up to 4 T. The GEM support structure was mounted on top of the readout plane described in section 2. Ten complete pad rows were read out with charge sensitive preamplifiers followed by a 12.5 MHz flash ADC system [13]. As counting gas, the so-called P5 mixture (95 % argon and 5 % methane) was used and the drift field was set to 90 V/cm in order to be —due to the velocity plateau at this value— independent from small drift field variations. The GEMs were used with voltages between 320 V and 325 V. Fields of 1.5 kV/cm were applied in the 2 mm wide transfer gaps, while a field of 3 kV/cm is used in the 3 mm wide induction region. With the used TPC prototype an effective gain measurement is not possible, but using the above mentioned parametrization [12] a gain of 10,000 can be estimated for the setup used here. Two scintillator counters —above and below the prototype— operated in coincidence were used to trigger on cosmic muons. More details about the trigger system and the whole setup can be found in [7].

The coordinate system used in the reconstruction is defined by the pad plane —x is pointing horizontally over the pad columns, while y follows the vertical rows— and the drift distance along the chamber axis, corresponding to the z axis.

The data reconstruction is divided in three steps. First, the pad-wise charge deposition from different time bins (corresponding to z values) is combined row-wise by a center of gravity method to three dimensional space points of charge, here denoted by hit. Second, a track finding algorithm is applied, which combines the hits to a track candidate. Finally, the tracks are fitted with an algo-

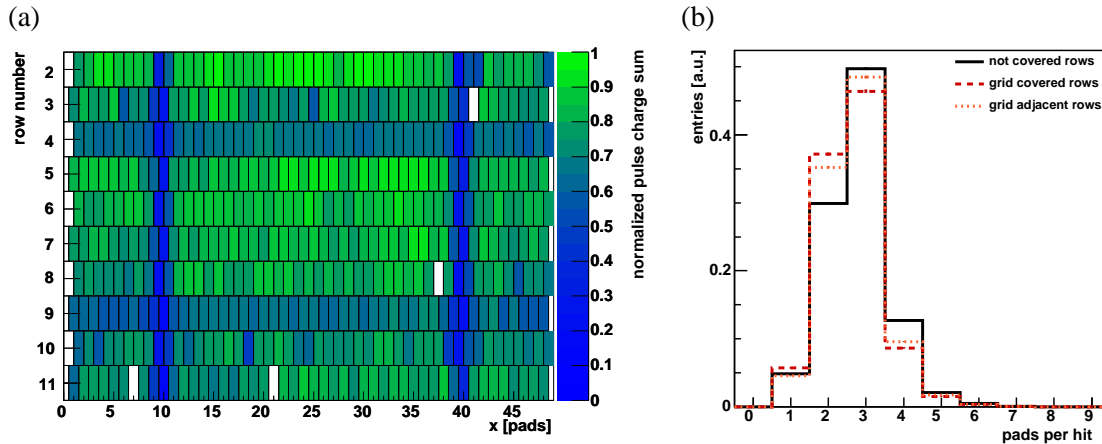


Figure 2. (a) Normalized charge sum —integrated over a measurement run— on the readout pads. In each row, pads 9, 10 and pads 39, 40 are covered partly by the vertical grid bars. The horizontal bars are positioned in row four and nine of the pad plane. (b) Influence of the horizontal grid bar on the number of pads contributing to a hit. The distribution has been normalized to the total number of entries. In both figures data measured at a magnetic field of 4 T are shown.

rithm assuming a circular path. More details about the reconstruction algorithms can be found in [14].

4. Grid Impact on Charge Measurement

The charge deposited on a single pad is the starting point for the reconstruction. Therefore the impact of the grid on the charge has been studied by investigating the total amount of charge deposited throughout a long data taking period with about 61,000 triggers. Assuming that the cosmic rays illuminate the TPC uniformly, any deviations from an uniform charge distribution is likely caused by the grid structure.

Figure 2(a) shows the normalized charge sum per pad integrated over a measurement run with about 61,000 triggers. The structure of the grid is clearly visible through regions of reduced overall charge. The vertical bars, going in the direction of increasing row numbers, cover large fractions of the pad underneath. Due to the staggering, on average close to 50 % of a pad in this region is covered by a grid bar. For the horizontal bars, oriented parallel to the x axis, the bars cover only one out of seven millimeters or about 15 %. The observed reduction in charge per pad is about 25 % for the horizontal bars, and 60 % for the vertical bars, which is in rough agreement with the assumption that the charge reduction is to the first order proportional to the geometrical area coverage through the grid.

The results show that a clear impact of the grid on the charge deposited on the pads exists. Most important is therefore the alignment of the vertical bars and the pad plane. The latter should have a staggered design to insure, that not a complete column of pads is shadowed by the grid. The horizontal bars should be aligned to the middle of a pad row in order to minimize their impact. For a large scale TPC the design of the support structure has to be adapted to the module layout to ensure that all pads are able to provide useful charge signals, which is desirable to preserve the

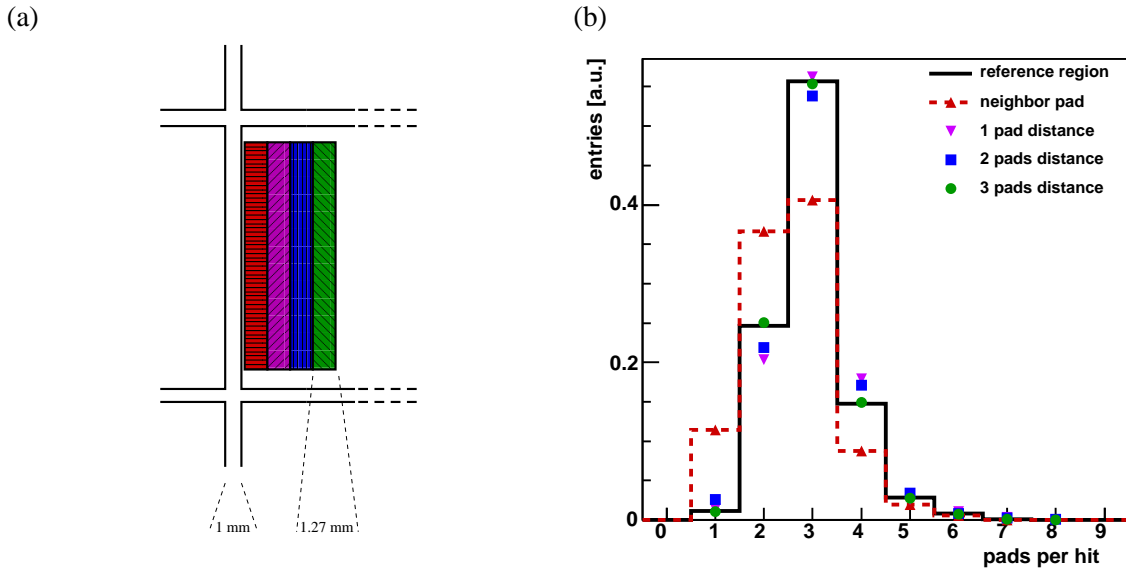


Figure 3. (a) Sketch of the neighboring vertical regions used for comparative studies of the influence of vertical grid bars. Each region has a width of 1.27 mm. (b) Influence of the vertical grid bar on the number of pads contributing to a hit for the different regions, measured at a magnetic field of 4 T. The distributions are normalized to the number of entries.

good pattern recognition performance of the TPC. In the following section, the impact on the hit reconstruction is studied.

5. Grid Impact on Hit Reconstruction and Hit Efficiencies

In this section, the impact of the grid on the number of pads with signals contributing to a hit and to the single hit efficiency is presented. More details like studies of the hit position, position uncertainty and the hit charge can be found in [11].

Hits are reconstructed within a row, as described in section 3. In figure 2(b) and 3(b) the average number of pads contributing to a hit is shown, studying the influence of horizontal (cf. figure 2(b)) and vertical (cf. figure 3(b)) grid bars. The solid histogram shows the distribution for hits which are located more than 5 mm away from a grid bar where the impact of the grid bar can be neglected. Hits reconstructed in an area of the pad plane where a pad is located below a grid are shown in the same plot in the dashed histogram, for an area covered by the horizontal bar in figure 2(b), for an area covered by the vertical bar in figure 3(b). In both cases, the average number of pads contributing to a hit is reduced. Close to the grid structure, more two-pad hits occur, which causes a larger uncertainty on the hit position when using a center of gravity method in the reconstruction [14].

To study how localized this effect is, hits with a center of gravity on pads directly adjacent to, or two or three pads away from, a covered pad are studied. For the horizontal bars, an effect is seen for the covered row (mean value of pads/hit distribution drops from 2.79 to 2.65) and a smaller effect for the adjacent row (mean value reduction only to 2.70). For the vertical bar as well, only hits on the directly adjacent region are strongly affected (mean value reduction for pad/hit distribution

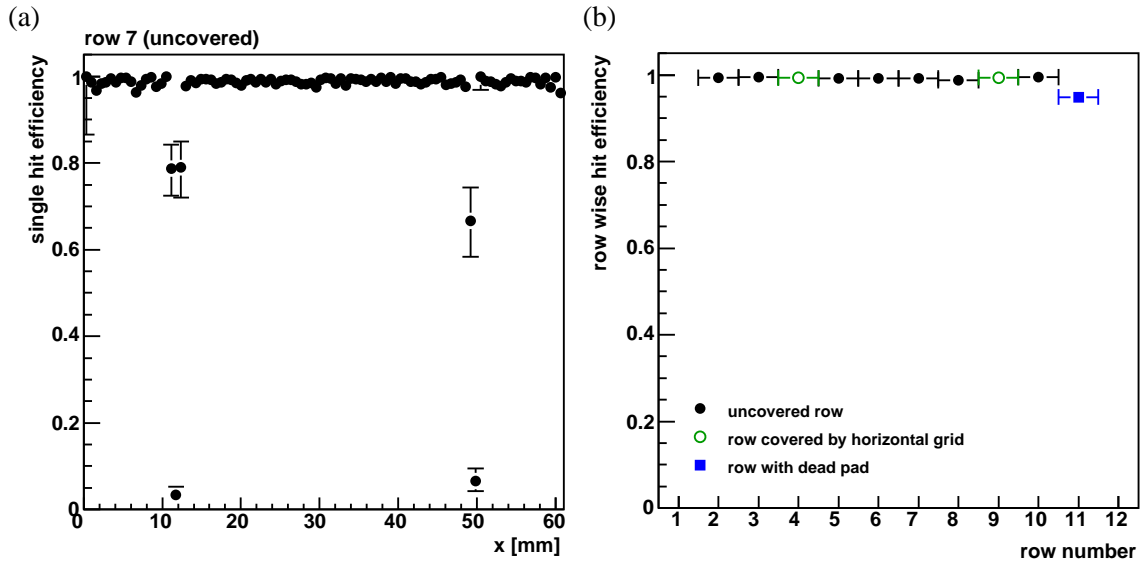


Figure 4. (a) Single hit efficiencies for a row not covered by a horizontal grid bar. The binning corresponds to half a pad pitch. (b) Single hit efficiency as function of the row number. An almost flat distribution can be observed. Only the last row has a slightly lower value due to dead pads in this row. All data measured at a magnetic field of 4 T.

from 2.96 in reference region to 2.55), while hits further away behave essentially as in the reference region (mean values for 1 pad distance: 3.05, 2 pads distance: 3.01, 3 pads distance: 2.96). Since the pad response function (PRF) has a width of 0.67-0.78 mm for different drift distances, it can be stated that hits occurring more than two widths of the PRF (one pad pitch) away from the grid structure are not influenced by it.

In the following, the efficiency to reconstruct a hit is calculated as the number of reconstructed hits relative to the expected number of hits at this position. The study was performed on a sample of about 42,000 single cosmic muon tracks. To determine the expected number of hits, tracks are searched for in the sensitive volume. The row for which the hit efficiency is investigated is excluded from the track finding and fitting. The expected hit position in the row under investigation is calculated from the parameters of the track. A hit reconstructed in this row is tagged as found if it is located within one pad width of the expected hit position.

With the used setup, tracks could have at most 10 rows contributing. To ensure a sample of well defined tracks, all rows except the one under investigation are required to show a hit on the track. The hit efficiency as a function of x for row seven (not influenced by a horizontal grid bar) is shown in figure 4(a). The binning is chosen such, that each bin corresponds to half a pad pitch, since the row wise staggering corresponds exactly to this half pad pitch. A drop in the efficiency is clearly visible for the x regions affected by the vertical grid bars, while the overall hit efficiency for this row can still be quoted with 98 % [11].

To study the effect of the horizontal bars, only tracks with neglectable curvature between the vertical bars are used. In figure 4(b) the hit efficiency is shown as a function of the row number, integrating over all x . The impact of the horizontal grids in row three and nine is negligible compared to the influence of a dead pad in row ten, which has a significantly lower intrinsic hit efficiency.

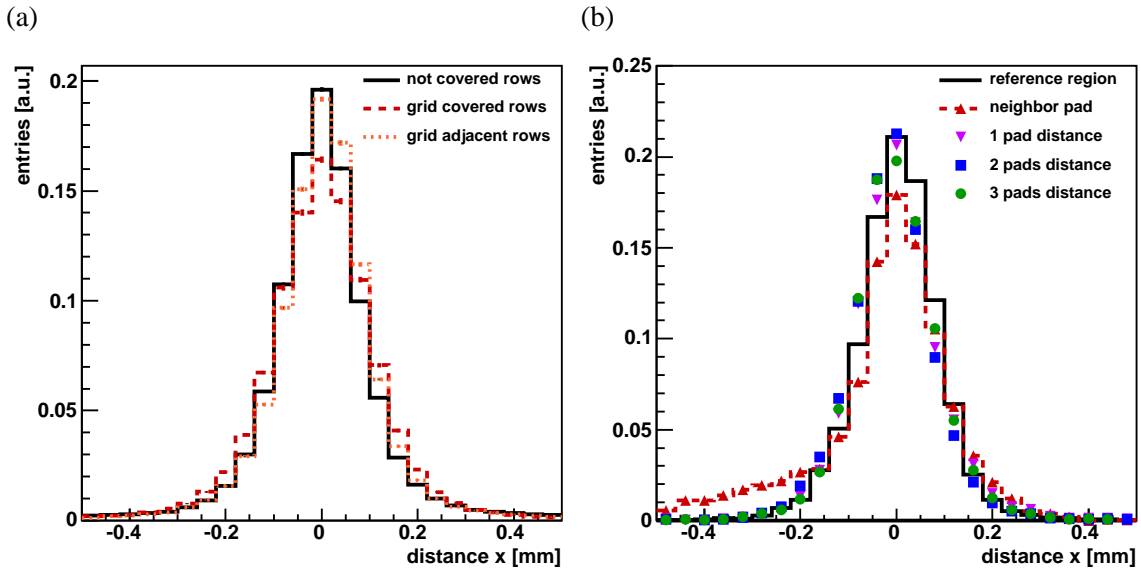


Figure 5. (a) Influence of a horizontal grid bar on the hit distance in x direction. (b) Impact of the vertical grid on the hit distance in x direction. Compared are regions with different distances to a vertical grid bar. All data measured at a magnetic field of 4 T. The distributions are normalized.

6. Impact of the Grid on the Track Reconstruction

186

Particle tracks are reconstructed from measured space points by fitting track parameters to these points. In this section, the impact of the grid structures on the point resolution and possible biases in the reconstruction of the points due to the grid are studied.

187

188

189

Distances Distances and residuals of hits describe the space between a hit and the corresponding fitted track. In the case of residuals, the actual hit is excluded from the fit, while for distances the hit is included in the fit. Residuals and distances are used to calculate the single point resolution with the help of the geometric mean method described in [14]. Here, only the impact of the grid on the distances is presented. The results for the residuals can be found in [11].

190

191

192

193

194

The uncertainty on the hit position for rows covered by a grid structure is larger, since the number of struck pads per hit is smaller. Consequently, these hits get smaller weights in the fitting procedure and are not able to pull the fitted track into their direction as much as hits with smaller uncertainties. In figure 5(a), as before, rows with three types of coverage are compared. As expected, the distances get larger for grid adjacent and grid covered rows.

195

196

197

198

199

To assess the impact of the vertical structures, the distribution of distances is shown for the reference sample and the four regions close to the vertical grid bar in figure 5(b). In contrast to the other distributions, the one for the adjacent region is not symmetric with respect to zero, the maximum is slightly shifted towards positive values of x and a tail is present on the negative side. The impact of the grid structure is that hit positions are artificially shifted away from the bars during the reconstruction. Since the number of tracks left to the grid bar (outer region of pad plane) is too low, only the region to the right of the grid bars are analyzed. That is the reason for the observable asymmetry in the distribution. The distance distributions of all other regions are symmetric, which

200

201

202

203

204

205

206

207

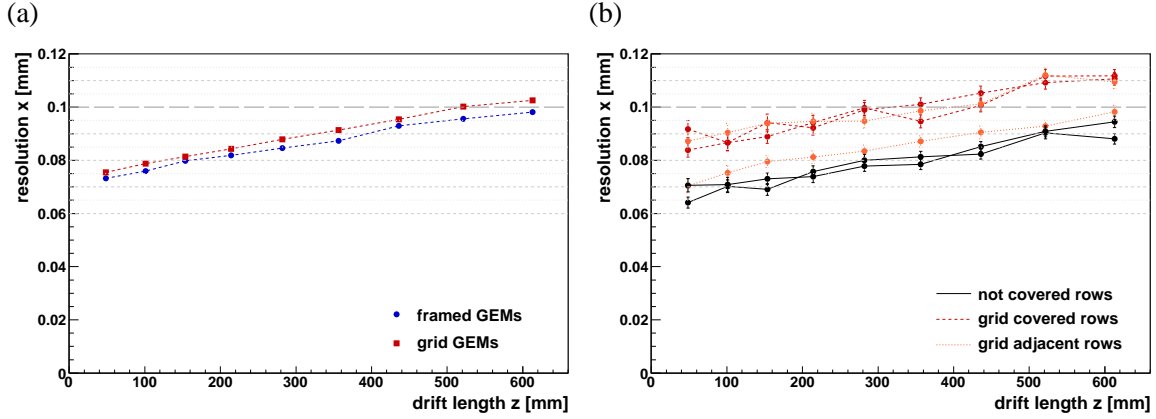


Figure 6. (a) Single point resolution as function of the drift length for a reference data set and a measurement run with grid GEMs at a magnetic field of 4 T. Both sets (grid/frame) were taken with the same field configuration and ten out of ten possible hits per track were required. (b) Influence of the horizontal grid bars on the single point resolution deduced by the χ^2 method including a pad response correction at a magnetic field of 4 T. Shown are single point resolutions as function of the drift length for six individual rows, two for each case of grid coverage. An impact of the vertical bars is avoided by excluding the outer x regions.

supports the assumption that the impact of the grid affects only hits located on directly adjacent pads and no further and broader shadowing effect takes place. 208
209

Single Point Resolution The single point resolution is of particular importance in tracking detectors. It eventually impacts the momentum resolution of a large scale TPC and gives a handle to judge the performance. 210
211
212

The single point resolution is determined with a χ^2 track fit method including pad response function (PRF) corrections. Details of this method and its implementation are given in [14]. The tracks 213

Table 3. Track cuts for single point resolution determination.

variable	requirement
number of tracks	$n_{\text{tracks}} = 1$
number of hits	$n_{\text{hits}} = n_{\text{rows}}$
x region	$2.54 \text{ mm} < x_{\text{hit}} < 59.06 \text{ mm}$
curvature	$ \kappa < 0.02 \text{ mm}^{-1}$
inclination in yz -plane	$ \theta < 0.45 \text{ rad}$
inclination in xy -plane	$ \phi < 0.1 \text{ rad}$

are selected according to the cuts summarized in table 3. 214

In figure 6(a), the single point resolution is shown for a reference run from a setup using framed GEMs compared with data obtained with grid GEMs. Both measurements were performed in a magnetic field of 4 T and with identical GEM settings. The differences between both measurements are small – about $5 \mu\text{m}$, which is in the range of normal run to run variations. 215
216
217
218
219

To draw a conclusion about the impact of the horizontal structures on the single point resolution, the effects of horizontal and vertical bars have to be disentangled. Hence, a cut on the x coordinate of hits is made to exclude the outer regions covered by the vertical bars. A safety distance of 220
221
222

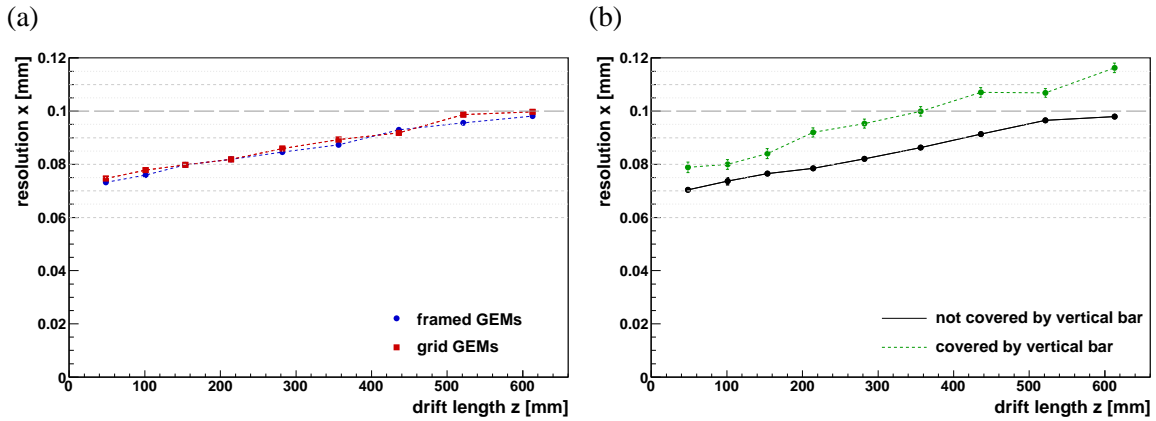


Figure 7. (a) Influence of the horizontal grid bars on the single point resolution as function of the drift length at a magnetic field of 4 T. The region in x is restricted to an area without vertical bars. (b) Single point resolution for regions covered by a vertical grid bar (dashed green) and x ranges, where no vertical bar is shadowing the pad plane (solid black), measured at a magnetic field of 4 T.

3 mm to the vertical bars has been chosen. For a detailed understanding of the impact of horizontal coverage, a comparison of row-wise calculated single point resolutions is presented in figure 6(b). A very clear distinction can be made between rows covered and not covered by the grid, almost 20 μm difference can be observed over the full drift length. The two rows adjacent to the grid show different results. The one closer to the horizontal bar, row ten (cf. figure 1(b)), is much more influenced than row three (almost half a pad height of distance), whose results are only slightly worse than those of the two reference rows.

A comparison of the single point resolution using all available ten rows, but with the same restriction on the x region, can be seen in figure 7(a). The results show that the horizontal bars have no influence on the measurement as a whole in terms of the single point resolution.

To illustrate the impact of vertical bars on the single point resolution, two sets of different regions of x are compared in figure 7(b). One set includes the x ranges around both vertical grid bars, while the other contains two reference areas of the same width, but uncovered by a vertical bar. Each area has a width of 8.62 mm: 1 mm for the bar itself and three pads to the left and to the right. The width of the areas is defined by the need to be close to the vertical bar in order to be sensitive to the effects and to be wide enough to have large enough statistics to gain reliable results. Furthermore, a certain width is needed to avoid an intrinsic ϕ cut in addition to the ϕ requirement from table 3. For this comparison, tracks with at least six out of ten hits are used. Six hits are needed to ensure stable track fits. Requiring more hits, would exclude tracks influenced by the grid.

A clear difference between the reference and the grid covered regions is visible. The deviations develop from 10 μm at short drift distances to almost 20 μm at the far end of the drift volume. In the case of the covered regions, less statistics is available increasing the uncertainties on the single point resolution.

To summarize the effect on the single point resolution, it can be stated that the overall resolution is not affected in a critical way. The impact of the vertical bars is as expected larger, compared to the one from the horizontal structures, which is negligible. For a large scale TPC, where many hits

per track are available, hits close to support structures can safely be excluded from the track fit and by this from the single point and momentum resolution determination, while still being used in the pattern recognition. In this way an efficient track finding can be ensured together with a precise determination of the track parameters.

7. Conclusion

A novel scheme to support and mount GEM foils inside a TPC has been developed. This self-supporting structure is made of a ceramic grid glued in between the GEM foils. Ceramic is well suited for applications in a gas amplification system due to its electrical and mechanical properties, since it is a good insulator and at the same time very stiff. The material budget can be reduced with respect to mounting GEMs on GRP frames. The new support structure allows a stable operation and has been successfully tested in a medium size TPC prototype.

In order to quantify the impact of the grid GEMs on the track reconstruction, cosmic muon tracks have been recorded in a magnetic field of 4 T. The data analysis has shown that the impact of the ceramic grid is visible in all steps of the track reconstruction due to a reduction of the measured charge. However, the impact of the bars perpendicular and parallel to the longer axis of a readout pad have to be treated separately. The horizontal structures do not affect the hit efficiency. The single point resolution obtained with grid GEMs covered by horizontal bars is competitive with results of previous GEM mounting methods. Vertical bars produce shifted hits in their immediate vicinity and the single point resolution is worsened by up to 20 % close to these structures.

The advantages of the developed grid support structure are the minimal amount of material, the achievable flatness without the need of stretching the foils, the almost edgeless module borders and the possibility to cover large areas without significant gaps. The developed grid mounting structure will enable the step from small GEM applications —used for proof-of-principle studies— to a large scale GEM TPC in a modern high energy detector like the ILD. As an intermediate step towards this goal, readout modules of size and design comparable to the one envisaged for a large scale TPC are being developed implementing the Grid GEM mounting. A first test has been performed with one module [15] in a large TPC prototype [16]. Based on these results, tests with an improved design are currently under way with three modules to show the applicability of the novel mounting structure under realistic conditions.

Acknowledgments

This work is supported by the Commission of the European Communities under the 6th Framework Programme 'Structuring the European Research Area', contract number RII3-026126.

References

- [1] T. Abe *et al.* [ILD Concept Group - Linear Collider Collaboration], *The International Large Detector: Letter of Intent*, arXiv:1006.3396 [hep-ex].
- [2] ILD Concept Group - Linear Collider Collaboration, *The International Large Detector: Detailed Baseline Document*, to be published in 2013.

[3] F. Sauli, *GEM: A new concept for electron amplification in gas detectors*, Nucl. Instrum. Meth. A **386** (1997) 531. 286
287

[4] Y. Giomataris, P. Rebourgeard, J. P. Robert and G. Charpak, *MICROMEGAS: A High granularity position sensitive gaseous detector for high particle flux environments*, Nucl. Instrum. Meth. A **376** (1996) 29. 288
289
290

[5] M. Chefdeville, H. van der Graaf, S. van der Putten, J. Timmermans, J. L. Visschers, P. Colas, Y. Giomataris and E. H. M. Heijne *et al.*, *An electron-multiplying 'Micromegas' grid made in silicon wafer post-processing technology*, Nucl. Instrum. Meth. A **556** (2006) 490. 291
292
293

[6] http://www.anceram.com/3_keramik/produktbeschreibung_en.php, *ANCeram Company website - technical ceramics*, 2010 294
295

[7] T. Lux, *Studies for a time projection chamber for the International Linear Collider and measurement of beauty cross sections in deep inelastic scattering at HERA*, DESY-THESIS-2005-019. 296
297

[8] F. Hegner, *private communication*, 2010 298

[9] <http://www.polytec-pt.com>, *Polytec PT company web site – in german*, 2010 299

[10] W. M. Yao *et al.* [Particle Data Group Collaboration], *Review of Particle Physics*, J. Phys. G **33** (2006) 1. 300
301

[11] L. Hallermann, *Analysis of GEM properties and development of a GEM support structure for the ILD Time Projection Chamber*, DESY-THESIS-2010-015. 302
303

[12] S. Lotze, *Ion Backdrift Minimisation in a GEM -Based TPC Readout*, PhD thesis, RWTH Aachen University. 304
305

[13] M. Ball, N. Ghodbane, M. E. Janssen and P. Wienemann, *A DAQ system for linear collider TPC prototypes based on the ALEPH TPC electronics*, LC-DET-2004-013, arXiv:0407.120 [physics] 306
307

[14] M. E. Janssen, *Performance studies of a time projection chamber at the ILC and search for lepton flavour violation at HERA II*, DESY-THESIS-2008-011. 308
309

[15] R. Diener, T. Behnke, S. Caiazza, I. Heinze, V. Pohl, C. Rosemann, O. Schafer and J. Timmermans *et al.*, *Beam Test with a GridGEM TPC Prototype Module*, arXiv:1202.6510 [physics.ins-det]. 310
311

[16] T. Behnke, K. Dehmelt, R. Diener, L. Hallermann, T. Matsuda, V. Pohl and P. Schade, *A Lightweight Field Cage for a Large TPC Prototype for the ILC*, JINST **5** (2010) P10011 arXiv:1006.3220 [physics.ins-det]. 312
313
314